RESEARCH ARTICLE





Coarsening droplets for frosting delay on hydrophilic slippery liquid-infused porous surfaces

Department of Mechanical Engineering, The University of Texas at Dallas, Richardson, Texas, USA

Correspondence

Xianming Dai, Department of Mechanical Engineering, The University of Texas at Dallas, Richardson, TX 75080, USA. Email: Dai@utdallas.edu

Funding information

Startup Funding by the University of Texas at Dallas; National Science Foundation Faculty Early Career Development Program, Grant/Award Number: 2044348; Army Research Office Young Investigator Program, Grant/Award Number: W911NF1910416

Abstract

Frosting occurs due to the freezing of condensed water droplets on a supercooled surface. The nucleated frost propagates through interdroplet bridges and covers the entire surface, resulting from the deposition of highly supersaturated vapor surrounding tiny droplets. While inhibition of the formation of frost bridges is not possible, the propagation of frost can be delayed by effectively removing tiny droplets. Passive technologies, such as superhydrophobic surfaces (SHS) and hydrophobic slippery liquid-infused porous surfaces (SLIPS), rely on static growth and direct contact with densely distributed droplets. However, use of these approaches in delaying frost propagation involves challenges, as the interdroplet distance remains small. Here, we report a new approach of spontaneous droplet movement on hydrophilic SLIPS to delay the formation of interdroplet frost bridges. Surface tension forces generated by the hydrophilic oil meniscus of a large water droplet efficiently pull neighboring droplets with a diameter of less than 20 µm from all directions. This causes a dynamic separation between water droplets and an adjacent frozen droplet. Such a process delays the formation and propagation of interdroplet frost bridges. Consequently, there is significant delay in frosting on hydrophilic SLIPS compared to those on SHS and hydrophobic SLIPS.

INTRODUCTION

Frosting is a natural phase-change phenomenon when moist air condenses and freezes on a cold surface.¹ This often results in problems that affect energy industries around the globe, causing substantial economic losses every year. For example, frosting on refrigerators and air conditioners can reduce their efficiency by 50%–70%.^{2,3} Additionally, it imposes a heavy burden on solar panels and causes mechanical damage to power transmission lines during the winter, resulting in prolonged power outages and severe risks

to human lives.⁴⁻⁶ Various active strategies, such as mechanical defrosting, electric heating, and de-icing chemicals, have been used to combat frosting.⁷⁻⁹ However, these approaches are energy-intensive and costly. Consequently, researchers have shifted their focus toward understanding the mechanism of the entire condensation-frosting process and adopting a passive approach to address the challenges in terms of frosting.

The condensation-frosting process primarily consists of three stages: frost nucleation, frost propagation, and frost accretion. ^{10,11} When vapor continually condenses on a substrate with a temperature

This is an open access article under the terms of the Creative Commons Attribution License, which permits use, distribution and reproduction in any medium, provided the original work is properly cited.

© 2024 The Authors. Droplet published by Jilin University and John Wiley & Sons Australia, Ltd.

below freezing, heterogeneous frost nucleation occurs at the interface between the droplet and the substrate by overcoming the Gibbs freeenergy barrier for heterogeneous nucleation. 12 Passive control of frost nucleation involves manipulating the interfacial free energy, interfacial geometry, and lattice structure match at the solid-liquid interface. 13-16 However, complete prevention of frost nucleation is challenging due to ubiquitous dust particles in the environment, which act as undesirable nucleation sites.¹⁷ Consequently, when a single droplet freezes, frost halos arise, which trigger the propagation of frost among adjacent droplets. 18 Frost propagation occurs through the formation of frost bridges that connect the condensates. 19,20 When a droplet freezes, the vapor pressure surrounding it becomes lower than that of the neighboring water droplets. At the same subcooling, the smaller water droplet has a higher supersaturation.^{21,22} This leads to localized vapor pressure gradients, where the frozen droplets act as local humidity sinks, capturing vapors from the neighboring water droplets. These vapors subsequently deposit as frost bridges and connect to the adjacent water droplets.²³ Soon after, frost propagates through a chain reaction, forming a network of interconnected bridges that covers the entire surface. The formation of these bridges relies on the interplay between the gap between droplets and the diameter of the water droplet being harvested.²⁴ In order to maintain mass conservation, the mass of the frost bridge deposited must be equivalent to the mass of the water droplet being collected. This relationship can be expressed using a dimensionless number known as the separation parameter

$$S^* = \frac{L_0}{d},\tag{1}$$

where L_0 is the distance from the edge of the frozen droplet to the center of the water droplet being harvested and d is considered as the initial diameter of the water droplet before being harvested.²⁴ There are two cases: (1) when the interdroplet gap is large such that the harvested water droplet completely evaporates, resulting in local bridge failure, that is, $S^* > 1$, and (2) when the interdroplet gap is small such that the frost bridge connects the harvested water droplet before complete evaporation, resulting in local bridge success, that is, $S^* < 1$. The criteria to delay frost propagation depend on delaying the formation of bridges by increasing the interdroplet gap. This can be accomplished through hygroscopic humidity sinks such as salty water, hygroscopic frost pattern, antifreeze chemicals, macroscale geometry with low ambient humidity, biphilic patterns, and accelerated jumping droplets. 25-33 However, these dry zones decay within a few minutes due to the gradual loss of the hygroscopic property by continuously harvesting water vapor from the ambient, leading to the nucleation of tiny droplets in the dry zones. 10 Therefore, it is important to continuously remove the highly supersaturated tiny water droplets during condensation. This can be achieved via coalescence-induced jumping on superhydrophobic surfaces (SHS) and sliding lateral movement on hydrophobic slippery liquid-infused porous surfaces (SLIPS).^{24,34-37} However, edge defects and droplet nucleation between the textures of SHS at high humidity lead to faster frost propagation, while condensed droplets on hydrophobic SLIPS remain confined within the lubricant layer in a closely packed

nature, resulting in fast frost propagation, with $S^* < 1$, locally. ^{38,39} Hence, continual and rapid removal of highly supersaturated tiny droplets is desired.

In this work, we show that spontaneous droplet climbing, that is, the coarsening effect, on a hydrophilic SLIPS can significantly delay heterogeneous frost nucleation by rapidly removing tiny water droplets, which effectively suppresses the growth of interdroplet bridges and delays frost propagation. This is achieved by a unique climbing mechanism of tiny droplets on the oil meniscus of a neighboring large droplet, leading to rapid droplet coalescence, removal, and rapid size evolution during condensation frosting. This creates large water-free areas and increases the interdroplet gaps, which delay the propagation of frost bridges, regardless of surface orientation, making it a promising approach compared to those on SHS and hydrophobic SLIPS. It is worth mentioning here that functional surfaces like SHS and SLIPS include micro/nanostructures and a lubricant layer, and durability has been a longstanding issue as they are prone to permanent damage, leading to accelerated frosting. 40,41 To tackle this issue, physical microstructures have been avoided in this study and the SLIPS were fabricated using durable quasi-liquid surfaces (QLS), which involves chemical grafting of flexible polymer chains. This eliminates the need for physical microstructures and has been demonstrated to be sustainable for bulk ice removal.42 We envision that our overall approach will provide a new paradigm for surface design to inhibit frost formation.

RESULTS AND DISCUSSION

We experimentally investigated frosting on a hydrophilic SLIPS with hydroxy-terminated polydimethylsiloxane (HPDMS) as the liquid lubricant with a thickness of 18.0 µm (Figure 1 and Supporting Information: Figures S1 and S2; refer to Methods section for details on sample preparation and setup). Our experiments were conducted in a humidity chamber, in which a Peltier cooling plate was set at -7°C and the relative humidity was maintained at 90%. When a water droplet is condensed on hydrophilic SLIPS, the elastocapillary effect causes each water droplet to be surrounded by an oil meniscus. 43 The length of the oil meniscus of a large droplet is longer than that of a tiny droplet. When two water droplets are close to one another with their oil menisci in contact, the greater surface tension force of the oil meniscus of the large droplet induces a spontaneous droplet movement. This leads to the mobility of tiny droplets toward the large droplet from all directions, resulting in immediate coalescence when they come into contact. Specifically, tiny droplets climb toward the neighboring larger droplet through its oil meniscus, while large droplets (d > 150 µm) move laterally along the surface. This phenomenon is known as the coarsening effect. 43 This meniscus-mediated spontaneous droplet climbing on hydrophilic SLIPS leads to rapid and efficient removal of highly supersaturated tiny droplets during condensation frosting. The interdroplet gap is thus sufficiently increased (Figure 1a), which restricts the local advancement of the frost bridge from the adjacent frozen droplet, resulting in delayed

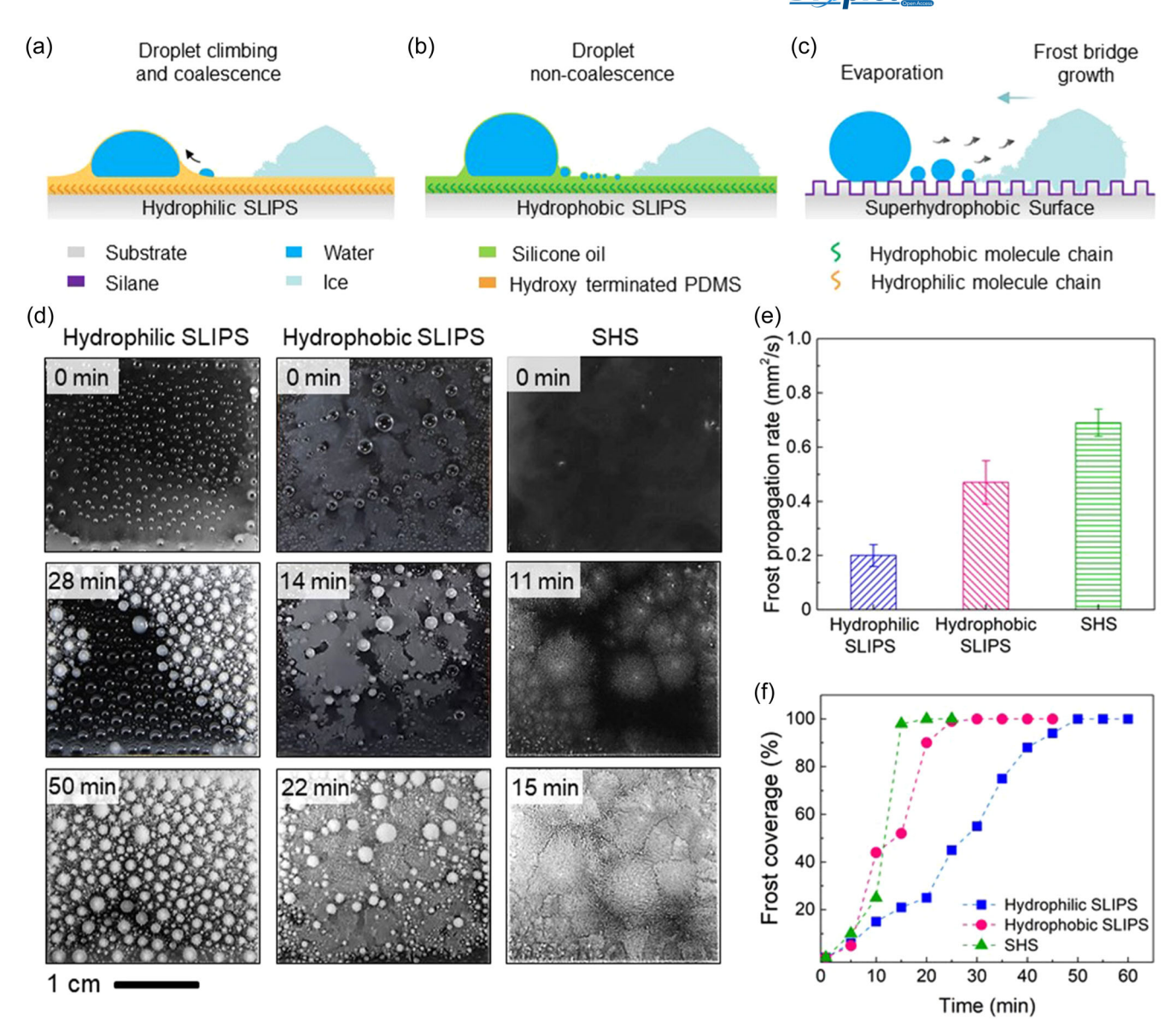


FIGURE 1 Meniscus-mediated spontaneous droplet movement and antifrosting performance. Schematics showing (a) droplet climbing and coalescence on hydrophilic slippery liquid-infused porous surfaces (SLIPS), (b) droplet noncoalescence on hydrophobic SLIPS, and (c) droplet renucleation after coalescence-induced jumping on superhydrophobic surfaces (SHS). (d) Time-lapse images showing condensation-frosting behavior on hydrophobic SLIPS, hydrophobic SLIPS, and SHS, (e) corresponding average frost propagation rate, and (f) percentage frost coverage. The onset of frost propagation on each substrate was marked as 0 min as shown in (d). PDMS, polydimethylsiloxane.

frost propagation. Comparatively, inefficient coalescence of droplets on a hydrophobic SLIPS (Figure 1b) and dense distribution of droplets on an SHS (Figure 1c) affected by edge defects result in faster propagation of frost.

To validate our hypothesis, we investigated the freezing delay potential of our hydrophilic SLIPS and compared its performance with a hydrophobic SLIPS and an SHS. All the test substrates (2.5 cm \times 2.5 cm) were cooled to –7°C under controlled environmental conditions of 20°C ambient temperature and 90% relative humidity. To ensure a fair comparison, the viscosities of the two SLIPS were in the same range (refer to Methods section for fabrication details and Supporting Information: Figure S1), and silicone oil was chosen as the

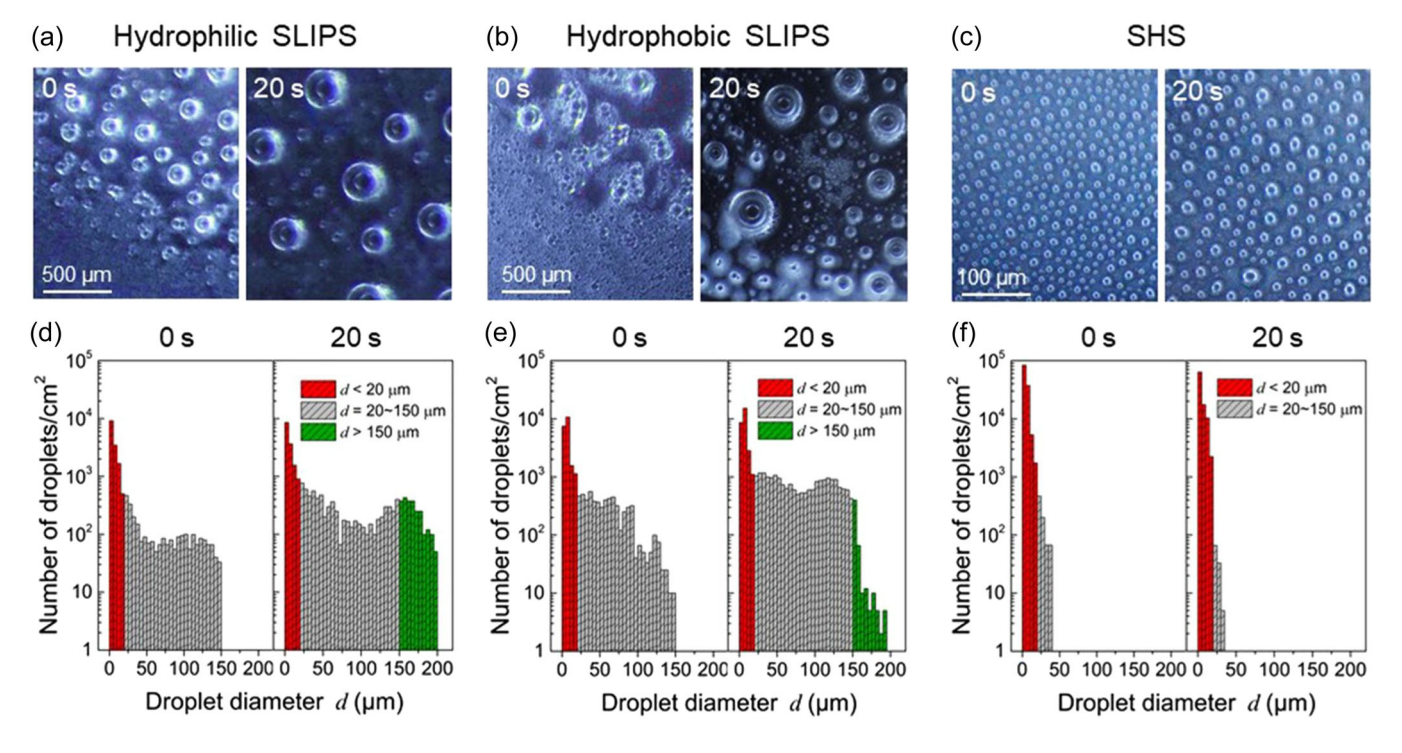
lubricant for hydrophobic SLIPS. The results of condensation-frosting experiments showed that the hydrophilic SLIPS lasted 2.7 and 3.5 times longer than the hydrophobic SLIPS and SHS, respectively, under high humidity conditions, with a significant difference in the frozen droplet size distribution (Figure 1d). The average frost propagation rate on the test surfaces was calculated by dividing the total surface area of each substrate by the time required for frost to cover the entire surface since the first frost occurrence. The frost propagation rate on hydrophilic SLIPS was 64% and 72% lower than that on the hydrophobic SLIPS and SHS, respectively (Figure 1e). The percentage frost coverage data in Figure 1f indicated that during the 5- to 11-min interval after the onset of frost propagation, frost

covered larger surface areas on the hydrophobic SLIPS with a faster propagation rate compared to both SHS and hydrophilic SLIPS. However, after 11 min, the SHS showed a faster propagation of frost compared to both hydrophobic SLIPS and hydrophilic SLIPS completely covering the surface within the next 5 min. The hydrophilic SLIPS took the longest time to reach complete frost coverage, which demonstrated that frosting could be significantly delayed by spontaneous droplet movement. To better understand the competition of frost propagation between the hydrophobic SLIPS and the SHS, we carried out a microscopic analysis of the test surfaces, described in the next section, during condensation frosting.

Before the occurrence of frost nucleation, we studied condensation at the microscale to observe the evolution of droplet size on the hydrophilic SLIPS compared to hydrophobic SLIPS and SHS (Figure 2). On the hydrophilic SLIPS, the meniscus-mediated spontaneous droplet movement resulted in a rapid coalescence of tiny droplets and evolution into large droplets immediately after droplet nucleation (Figure 2a). On the contrary, droplets nucleated within the lubricant layer on the hydrophobic SLIPS, which resulted in low droplet mobility, leading to slow and inefficient coalescence (Figure 2b). The SHS is covered by several renucleated tiny droplets after the removal of larger droplets by coalescence-induced jumping (Figure 2c). On the hydrophilic SLIPS, the coarsening effect increases the number of large droplets within a short span of 20 s due to the continuous climbing and coalescence of tiny droplets (Figure 2d). On the hydrophobic SLIPS,

The uniqueness of the frosting mechanism on hydrophilic SLIPS is that it could spontaneously remove tiny droplets from the vicinity of the frozen droplets due to the surface tension force of the oil meniscus of the adjacent large droplet. Figure 3a shows the frost propagation dynamics on hydrophilic SLIPS at the microscopic scale compared to hydrophobic SLIPS with tiny droplets confined within the lubricant layer (Figure 3b) and SHS with closely packed droplets (Figure 3c). Within the next 4 min, frosting covered the SHS entirely in the field of view, but mobile droplets on the hydrophobic SLIPS delayed frosting compared to SHS. However, due to the thick wrapping layer of lubricant, droplet mobility on the hydrophobic SLIPS was inefficient, resulting in the packing of tiny droplets. This caused frosting to propagate among these packed droplets, resulting in only a small frost-free area on the hydrophobic SLIPS (Supporting

those on hydrophilic SLIPS.



Droplet size distribution on different surfaces. Microscopic image of droplet size distribution on (a) hydrophilic slippery liquidinfused porous surfaces (SLIPS), (b) hydrophobic SLIPS, and (c) superhydrophobic surfaces (SHS). Number of droplets on (d) hydrophilic SLIPS showing evolution of tiny droplets ($d < 20 \,\mu\text{m}$) to intermediate-size ($d = 20-150 \,\mu\text{m}$) and large droplets ($d > 150 \,\mu\text{m}$), (e) hydrophobic SLIPS showing an increase in tiny as well as intermediate-size droplets ($d = 20-150 \, \mu \text{m}$) but not on large droplets, and (f) SHS showing evolution of tiny droplets and decrease in the intermediate-size droplets due to coalescence-induced jumping.

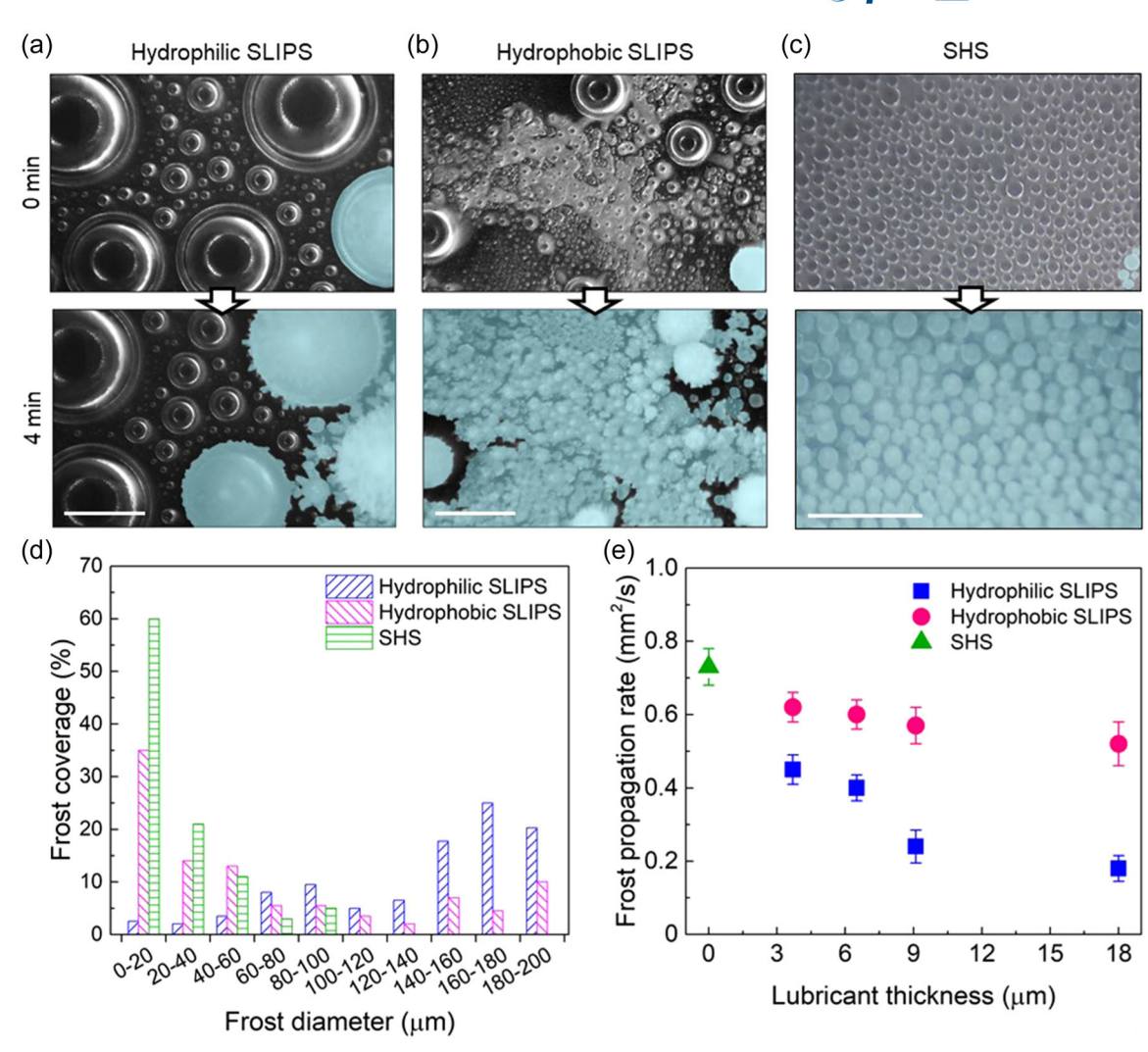


FIGURE 3 Frost propagation on different surfaces. Microscopic images showing time-lapse condensation frosting on (a) hydrophilic slippery liquid-infused porous surfaces (SLIPS), (b) hydrophobic SLIPS with fast propagation due to tiny droplets confined within the lubricant layer, and (c) superhydrophobic surfaces (SHS) with closed packing of tiny droplets. Here, 0 min depicts the occurrence of the first frozen droplet in the field of view of the microscope. Pale blue color is used to depict frost. (d) Percentage frost coverage showing frost size distribution and (e) optimization of the frost propagation rate with varying lubricant thicknesses. Scale bar: 200 μm.

Information: Movie S1). Meanwhile, within the same period of 4 min, frost could propagate only less than 50% on the hydrophilic SLIPS under the field of view of the microscope with sufficient frost-free area. This is due to the efficient removal of tiny droplets by spontaneous droplet movement resulting in an increased interdroplet gap. After the entire surface was covered with frost, as can be seen from the frost distribution shown in Figure 3d, the hydrophilic SLIPS had the lowest percentage of tiny frozen droplets at less than 5%, whereas in hydrophobic SLIPS, more than 35% of the surface was covered with tiny frozen droplets due to their restricted mobility owing to confinement within the lubricant layer. SHS had a staggering 60% surface coverage with tiny frozen droplets due to the existence of numerous tiny droplets. The frost distribution plot also showed a variation in the number of large frozen droplets on these surfaces due to their distinct condensation-frosting behavior. The hydrophilic SLIPS showed the maximum coverage by large frozen

droplets at almost 60% due to the rapid evolution of droplets by spontaneous movement during condensation frosting. However, hydrophobic SLIPS showed 23% coverage of large droplets due to the inefficient evolution of droplets, and SHS had no large droplets due to coalescence-induced jumping. This microscopic study indicates that the initial frosting competition between hydrophobic SLIPS and SHS is due to the packing of tiny droplets on hydrophobic SLIPS resulting from a thick wrapping layer of lubricant. This also affects the droplet size distribution during condensation frosting on the hydrophobic SLIPS, resulting in faster frost propagation compared to hydrophilic SLIPS.

The rate of frost propagation on the hydrophilic SLIPS could be optimized by increasing the thickness of the lubricant layer. As HPDMS has low thermal conductivity (~0.15 Wm⁻¹ K⁻¹), a thicker lubricant layer on the hydrophilic SLIPS would essentially provide better thermal resistance. However, the increased lubricant thickness

improves the average coarsening speed and the oil meniscus length. 43 A larger oil meniscus length on a thicker hydrophilic SLIPS results in a stronger interfacial tension force, which enables tiny droplets to climb faster and coalesce with the neighboring large droplet. This could effectively remove a larger area of tiny droplets to increase the interdroplet gaps. To quantify the impact of spontaneous droplet movement on condensation frosting, we measured the frost propagation rates and the corresponding coarsening speed on both hydrophilic SLIPS and hydrophobic SLIPS with varying lubricant thicknesses (Figure 3e and Supporting Information: Figure S3). We used different spin speeds of 8000, 4000, 2000, and 1000 rpm to set the lubricant thicknesses to 3.0, 6.5, 9.0, and 18.0 µm, respectively. On hydrophobic SLIPS, the frost propagation rate decreased slightly from 0.62 to 0.57 mm² s⁻¹ when lubricant thickness was increased from 3.0 to 18.0 µm (Figure 3e). However, the frost propagation rate decreased significantly from 0.45 to 0.18 mm² s⁻¹ on hydrophilic SLIPS when the lubricant thickness was increased from 3.0 to 18.0 µm (Figure 3e and Supporting Information: Movie S2), with an increase of 175% in the coarsening speed. With an identical lubricant thickness, hydrophilic SLIPS showed a slower frost propagation rate than hydrophobic SLIPS due to stronger spontaneous movementinduced rapid droplet removal leading to the increased interdroplet gap, while SHS showed the fastest average frost propagation rate of 0.75 mm² s⁻¹ among the three surfaces.

Frosting on hydrophilic SLIPS involves a dynamic process where the tiny droplets are not static but move from their initial position, climb on the oil meniscus of a neighboring large droplet, and eventually coalesce with it. This is different from the frosting on SHS where the tiny droplets remain static at the position of their nucleation, L_0 (Figure 4a). The existing model in Equation (1) is based on droplet evaporation and its deposition as a frost bridge. There is either local bridging success on the SHS if the interdroplet gap is small ($S^* < 1$), such that the frost bridge connects the droplet before its complete evaporation, or local bridging failure if the interdroplet gap is large ($S^* > 1$), such that the droplet evaporates completely before the frost bridge can connect. However, on hydrophilic SLIPS, there is a local bridging failure even with an initial small interdroplet gap ($S^* < 1$) as the droplet is not static but moves away from the frost bridge (Supporting Information: Movie \$3). Consequently, the interdroplet gap increases dynamically as the droplet starts to move. This limits the validity of the existing scaling model to a static process because it cannot accurately predict the local bridging failure for a dynamic process such as the hydrophilic SLIPS. Hence, we proposed a dynamic model by introducing parameters for droplet mobility into the existing evaporation model. A dynamic separation parameter, S, has been introduced to characterize the dynamic interdroplet gap on a hydrophilic SLIPS when a tiny droplet just starts to move by a distance d at a critical time t_c

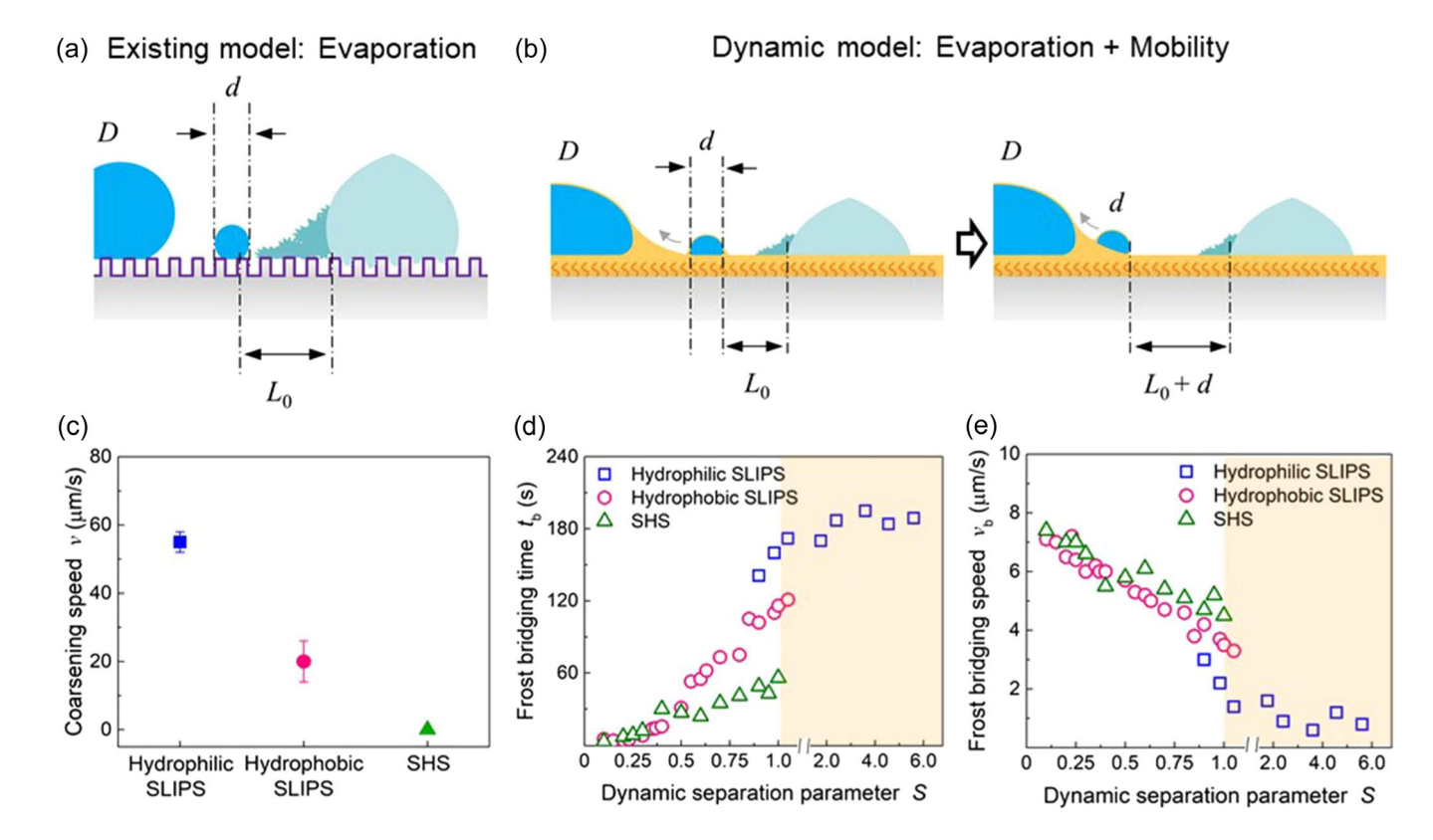


FIGURE 4 Dynamic interdroplet gap. Schematics showing (a) the existing model and (b) the new proposed model to characterize separation parameters. (c) Average coarsening speed on different surfaces and corresponding bridging dynamics showing (d) frost bridging time and (e) frost bridging speed in relation to the separation parameter. SHS, superhydrophobic surfaces; SLIPS, slippery liquid-infused porous surfaces.

on Wiley Online Library for rules of use; OA

are governed by the

$$S \sim \frac{L_0}{d} \left(1 + \frac{v_c}{v_b} \right) \begin{cases} v > v_c, & \text{frosting prevention,} \\ v_c \ge v > 0, & \text{frosting delay,} \\ v = 0, & \text{existing model,} \end{cases}$$
 (2)

where v is the average coarsening speed, v_c is the critical droplet speed at which the tiny droplet has moved a distance d and starts climbing on the oil meniscus, and v_b is the frost bridging speed. Under the limiting condition when the tiny droplet starts to move with a critical speed v_c, the frost bridge may either form or not. As the droplet moves a distance d away from its initial gap, L_0 , it instantaneously disappears by coalescing with a neighboring large droplet through the coarsening effect. Therefore, the dynamic interdroplet gap can be represented as $L_t = L_0 + d$ (Figure 4b). Considering that mass is conserved under the limiting condition of critical time t_c , the rate of evaporation of the tiny droplet being harvested by the frozen droplet should be equivalent to the mass rate of deposition of a frost bridge during droplet mobility (see the derivation in Supporting Information: Figure \$4). Frosting behavior may vary with the coarsening speed v_1 as: (1) When $v > v_c$, frosting can be potentially prevented due to the increase in the dynamic interdroplet gap as in the case of hydrophilic SLIPS. (2) When $v_c \ge v > 0$, frosting can be delayed as the droplet is just mobile as in the case of hydrophobic SLIPS. (3) On the contrary, when v = 0, the tiny droplet remains static. This is the same condition as that in the existing evaporation model, where there is no dynamic motion of the droplet and thus, $L_t = L_0$. Therefore, when v = 0, local bridging success or failure depends solely on the evaporation of the droplet, which influences the static interdroplet gap, L_0 .

The average coarsening speed on a hydrophilic SLIPS due to spontaneous droplet movement is calculated to be approximately three times larger than that on hydrophobic SLIPS, while SHS did not have a coarsening speed because of the lack of a lubricant layer (Figure 4c). The bridge formation dynamics on hydrophilic SLIPS compared to hydrophobic SLIPS and SHS is shown in Figure 4d,e, where S > 1 indicates local bridging failure, while S < 1indicates local bridging success. The time required for bridge formation on hydrophilic SLIPS was longer compared to that for hydrophobic SLIPS and SHS. In general, spontaneous droplet movement on the hydrophilic SLIPS significantly increased the dynamic interdroplet gap (S > 1), resulting in local bridge failure. After the tiny droplet climbed and coalesced with the neighboring large droplet, this large droplet and the frosted droplet became the new local frost-droplet system. Assuming no lateral movement of the large droplet, the time required for the frost bridge to reach the large droplet was considered as the frost bridging time for a visual comparison in Figure 4d, and the corresponding frost bridging speeds are shown in Figure 4e. The proposed model considering droplet mobility along with evaporation is more comprehensive than the existing model as it can predict bridging success and failure for both static and dynamic frosting processes.

Spontaneous droplet movement on hydrophilic SLIPS proved beneficial for frosting delay by efficient and rapid removal of tiny droplets (Figure 5a). This created local regions of S > 1 as the

interdroplet gap increased dynamically (Figure 5b). Meanwhile, droplet sizes evolved due to the continuous rapid climbing and coalescence of tiny droplets into larger ones, increasing their sizes. These larger droplets moved laterally along the surface of the hydrophilic SLIPS (Figure 5c). Due to the random lateral movement, such large droplet mobility is detrimental as it could result in contact with a neighboring frozen droplet and eventually freeze (Figure 5d and Supporting Information: Movie \$4). With the induced freezing of large droplets due to their lateral movement, a large portion of the surface area on the hydrophilic SLIPS could be covered by frost eventually, leading to the failure of complete frosting prevention. Directional transport of large water droplets is beneficial for several circumstances like draining away from the surface and controlling droplet mobility by anchoring it using patterned SLIPS. 44,45 Therefore, if the patterned SLIPS is well designed to control the mobility of the large droplets, there is a potential to delay frost propagation more effectively compared to the flat SLIPS.

The delayed frost propagation on hydrophilic SLIPS through the rapid removal of tiny droplets occurs regardless of the surface orientation. However, horizontal alignment showed a longer delay in the freezing process than vertical alignment (Figure 5e,f and Supporting Information: Movie \$5). In the vertical alignment, the large droplets shed fast on the hydrophilic SLIPS, so they have a high likelihood of connecting with frost and freezing themselves. Here, we emphasize that low contact angle hysteresis (CAH) is not a decisive factor for frost propagation. To confirm this point, we compared the condensation frosting process of hydrophilic SLIPS in vertical alignment with that of a QLS and a hydrophobic surface (silane) with CAH of 2°, 1°, and 8.7°, respectively. The QLS with the ultralow CAH of 1° was fabricated using the vapor-phase method described in our previous work.⁴⁶ The experimental data revealed that the hydrophilic SLIPS delayed frosting 2.4 and 2.9 times longer than the QLS and silane coatings, respectively (Supporting Information: Figure \$5a). Correspondingly, the frost propagation rate on hydrophilic SLIPS was 67% and 71% slower than that on QLS and silane (Supporting Information: Figure \$5b). The fact that frost covered the QLS faster than the hydrophilic SLIPS confirms that the spontaneous droplet movement on hydrophilic SLIPS is a new mechanism that leads to longer delay of frost propagation.

CONCLUSION

In summary, we have demonstrated a new mechanism of spontaneous droplet movement on hydrophilic SLIPS to delay frost propagation by the rapid removal of tiny droplets with high supersaturation. These tiny droplets spontaneously climb on the oil meniscus of a neighboring large droplet, dynamically increase the interdroplet gap, and significantly inhibit the formation of frost bridges. To support this finding, we have proposed a comprehensive model for dynamic interdroplet gaps to characterize the local success and failure of frost bridging. Condensation frosting was studied on hydrophilic SLIPS for the first time and shown to be delayed compared to SHS and

(a) Tiny droplet climbing delays bridging (b) Us State of the state o

FIGURE 5 Bridging behavior with droplet evolution on hydrophilic slippery liquid-infused porous surfaces (SLIPS). (a) Schematic and (b) microscopic images showing bridging delay with spontaneous droplet movement. (c) Schematic and (d) microscopic images showing bridging success with lateral movement of large droplets. Scale bar: 200 μm. Time-lapse images showing comparison of condensation frosting in (e) horizontal alignment and (f) vertical alignment.

hydrophobic SLIPS through the continuous removal of tiny droplets limiting frost bridge propagation. This study offers a new avenue for developing effective strategies to combat frosting propagation. We envision that immobilizing the randomly moving large droplets can reduce their chances of nucleation, resulting in longer delay of complete frost coverage on the entire surface.

METHODS

Materials: Polydimethylsiloxane hydroxy-terminated (viscosity: 16–32 cSt), polydimethylsiloxane trimethylsiloxy-terminated (silicone oil) (viscosities: 20 and 500 cSt), and (tridecafluoro-1,1,2,2-tetrahydrooctyl) trichlorosilane (98%) were purchased from Gelest. n-Heptane (99%) was purchased from Sigma-Aldrich and toluene (99.5%) from VWR. Silicon (Si) wafers <100> p-type (diameter: 4 in.) were purchased from University Wafer. Polycarbonate blocks and

sheets were purchased from McMaster-Carr to fabricate the humidity chamber for condensation-frosting experiments.

Fabrication of hydrophobic SLIPS and corresponding QLS: The fabrication process of QLS was exactly the same as that in our previously published work. Flexible polymers of methyl-terminated polydimethylsiloxane (i.e., silicone oil) (viscosity: 500 cSt) were tethered on a solid substrate using a one-step self-catalyzed grafting method through immersion in a solvent mixture of silicone oil and *n*-heptane at the ratio of 1:10. The substrates were immersed in the solution mixture for 48 h, followed by rinsing with toluene to remove the visible lubricant layer from the surface. Specifically, the siloxane-grafted substrates with the excess lubricant on the surface were immersed in a toluene bath and placed inside a shaker at 100 rpm for 2 min to ensure uniform rinsing. To make the hydrophobic SLIPS, the siloxane-grafted substrates were spin-coated at 30 s with silicone oil (viscosity: 20 cSt) to the desired lubricant thickness (Supporting Information: Figure S1a).

Fabrication of hydrophilic SLIPS: A substrate with abundant activation sites (–OH group) was immersed in a pool of polydimethylsiloxane hydroxy-terminated (hydroxy-PDMS) (viscosity: $16-32\,\text{cSt}$) overnight while being heated at a temperature of 50°C on a hot plate (Supporting Information: Figure S1b). This allowed polymer brushes of hydroxy-PDMS to be grafted on the substrate, which facilitated stable locking of the lubricant between the grafted molecule chains. The immersed substrates were then optimized to the desired lubricant thickness using a spin-coater (30 s) to make the hydrophilic SLIPS. Specifically, four spin speeds of 8000, 4000, 2000, and 1000 rpm were implemented to develop hydrophilic SLIPS with lubricant thicknesses of 3.7, 6.5, 9.0, and $18.0\,\mu\text{m}$, respectively. All substrates in this study were oxygen plasma-treated for $10\,\text{min}$ at $200\,\text{W}$ with $200\,\text{mTorr}$ O_2 gas before immersion-based surface fabrication.

Fabrication of SHS: A cleaned Si wafer was immersed in a solution of 4.8 M hydrofluoric acid (HF) and 0.01 M silver nitrate (AgNO $_3$) for 1 min to deposit catalysts. The silver ions (Ag $^+$) were reduced to Ag nanoparticles, which deposited on the Si surfaces and acted as catalysts to enhance local etching. The wafer with a catalyst was then placed in the etching solution containing 4.8 M HF and 0.3 M hydrogen peroxide (H $_2$ O $_2$) for 4 min, which yielded a 1 μ m depth of the nanostructures. After etching, the wafers were immersed in a 30% diluted nitric acid (HNO $_3$) solution to dissolve the Ag nanoparticles. Then, the wafer was washed with deionized water and dried with nitrogen gas. Finally, the nanostructured black Si was salinized by (tridecafluoro-1,1,2,2-tetrahydrooctyl) trichlorosilane in the vapor phase to make the SHS.

CAH measurements: The CAH measurements were carried out using a standard goniometer (Model 290; Ramé-Hart) at room temperature under ambient conditions (20–22°C, ~40% relative humidity). For the measurement of CAH, the surface was tilted relative to the horizontal plane until the liquid droplet started to slide along the surface. Then, the advancing and the receding contact angles of the droplet were calculated using a computer program in which the drops were fitted into a spherical cap. All the advancing and receding contact angle values were averaged from at least five independent measurements by applying ~5 μL droplets on the test surfaces.

Experimental setup: The tests for antifrosting were performed using a custom-built setup (Supporting Information: Figure S2). All experiments were performed in an environment with an ambient temperature of $20\pm1^{\circ}\text{C}$ and relative humidity of $90\pm2\%$. The samples were placed on a Peltier stage maintained at a temperature of -7°C and held under a $\times20$ microscope. The resulting condensation frosting was captured with a digital camera. Time zero in Figures 1 and 3 corresponds to the first moment of frost nucleation on a substrate. The frost propagation rate was approximated as the total surface area of the substrate divided by the time required for frost to propagate and completely cover the entire surface. Three fresh samples each of hydrophilic SLIPS, hydrophobic SLIPS, and SHS were used at the given temperature of -7°C to obtain uncertainties within a 95% confidence limit for the overall frost propagation.

Image processing: To characterize condensation-frosting events, the diameters of all condensed droplets and the interdroplet gaps in the field-of-view of the microscope were manually measured using ImageJ along with the percentage surface frost coverage. Surface frost coverage images were captured at different time stamps, and then they were transformed into black and white using the Threshold tool in ImageJ, where white pixels represented the frost-covered areas. The area of white pixels was divided by the total pixel area of each image to calculate the percentage of surface frost coverage. The droplet size distribution was calculated from screenshots of original videos by utilizing the Threshold and the Analysis tools in ImageJ. Coarsening speed and bridging speed were also calculated using ImageJ by measuring the distances covered in a certain time. The standard deviation was calculated based on three independent

ACKNOWLEDGMENTS

measurements for each case.

J. S. and X. D. gratefully acknowledge the startup funding provided by the University of Texas at Dallas. D. M. and X. D. acknowledge the National Science Foundation Faculty Early Career Development Program (Award No. 2044348). Z. G. and X. D. acknowledge the Army Research Office Young Investigator Program (Award No. W911NF1910416).

CONFLICT OF INTEREST STATEMENT

The authors declare no conflict of interest.

ORCID

Zongqi Guo http://orcid.org/0000-0002-9567-837X

Xianming Dai http://orcid.org/0000-0001-5050-2867

REFERENCES

- 1. Yang S, Wu C, Zhao G, et al. Condensation frosting and passive antifrosting. *Cell Rep Phys Sci.* 2021;2:100474.
- Yu J, Zhang H, You S. Heat transfer analysis and experimental verification of casted heat exchanger in non-icing and icing conditions in winter. *Renew Energy*. 2012;41:39-43.
- Huang L, Liu Z, Liu Y, Gou Y, Wang J. Experimental study on frost release on fin-and-tube heat exchangers by use of a novel antifrosting paint. Exp Therm Fluid Sci. 2009;33:1049-1054.
- Fillion RM, Riahi AR, Edrisy A. A review of icing prevention in photovoltaic devices by surface engineering. Renew Sustain Energy Rev. 2014;32:797-809.
- Chang SE, McDaniels TL, Mikawoz J, Peterson K. Infrastructure failure interdependencies in extreme events: power outage consequences in the 1998 ice storm. Nat Hazards. 2007;41:337-358.
- Laforte J-L, Allaire MA, Laflamme J. State-of-the-art on power line de-icing. Atmos Res. 1998;46:143-158.
- Egbert RI, Schrag RL, Bernhart WD, Zumwalt GW, Kendrew TJ. An investigation of power line de-icing by electro-impulse methods. *IEEE Trans Power Deliv.* 1989;4:1855-1861.
- Tan H, Tao T, Xu G, Zhang S, Wang D, Luo X. Experimental study on defrosting mechanism of intermittent ultrasonic resonance for a finned-tube evaporator. Exp Therm Fluid Sci. 2014;52:308-317.
- Wang K, Nelsen DE, Nixon WA. Damaging effects of deicing chemicals on concrete materials. Cem Concr Compos. 2006;28:173-188.
- Nath S, Ahmadi SF, Boreyko JB. A review of condensation frosting. Nanoscale Microscale Thermophys Eng. 2017;21:81-101.

- 11. Gu T, Zhao Y, Liu Y, Wang D. A review of condensation frostingmechanisms and promising solutions. Crystals. 2023;13:493.
- Jung S, Tiwari MK, Doan NV, Poulikakos D. Mechanism of supercooled droplet freezing on surfaces. Nat Commun. 2012;3:615.
- Fitzner M, Sosso GC, Cox SJ, Michaelides A. The many faces of heterogeneous ice nucleation: interplay between surface morphology and hydrophobicity. J Am Chem Soc. 2015;137:13658-13669.
- Schutzius TM, Jung S, Maitra T, et al. Physics of icing and rational design of surfaces with extraordinary icephobicity. Langmuir. 2015; 31:4807-4821.
- Carrasco J, Michaelides A, Forster M, Hag S, Raval R, Hodgson A. A one-dimensional ice structure built from pentagons. Nat Mater. 2009:8:427-431.
- Eberle P, Tiwari MK, Maitra T, Poulikakos D. Rational nanostructuring of surfaces for extraordinary icephobicity. Nanoscale. 2014;6:4874-4881.
- Bai G, Gao D, Liu Z, Zhou X, Wang J. Probing the critical nucleus size for ice formation with graphene oxide nanosheets. Nature. 2019; 576:437-441
- Jung S, Tiwari MK, Poulikakos D. Frost halos from supercooled water droplets. Proc Natl Acad Sci USA. 2012;109:16073-16078.
- Dooley JB. Determination and Characterization of Ice Propagation Mechanisms on Surfaces Undergoing Dropwise Condensation. PhD thesis. Texas A&M University; 2010.
- Guadarrama-Cetina J, Mongruel A, González-Viñas W, Beysens D. Percolation-induced frost formation. Europhys Lett. 2013;101:16009.
- Korolev A, Isaac G. Phase transformation of mixed-phase clouds. O J R Meteorol Soc. 2003:129:19-38.
- Chavan S, Park D, Singla N, Sokalski P, Boyina K, Miljkovic N. Effect of latent heat released by freezing droplets during frost wave propagation. Langmuir. 2018;34:6636-6644.
- Nath S, Boreyko JB. On localized vapor pressure gradients governing condensation and frost phenomena. Langmuir. 2016;32:8350-8365.
- Boreyko JB, Collier CP. Delayed frost growth on jumping-drop superhydrophobic surfaces. ACS Nano. 2013;7:1618-1627.
- Guadarrama-Cetina J, Mongruel A, González-Viñas W, Beysens D. Frost formation with salt. Europhys Lett. 2015;110:56002.
- 26. Boreyko JB, Hansen RR, Murphy KR, Nath S, Retterer ST, Collier CP. Controlling condensation and frost growth with chemical micropatterns. Sci Rep. 2016;6:19131.
- Sun X, Rykaczewski K. Suppression of frost nucleation achieved using the nanoengineered integral humidity sink effect. ACS Nano. 2017;11:906-917.
- Yao Y, Zhao TY, Machado C, Feldman E, Patankar NA, Park K-C. Frost-free zone on macrotextured surfaces. Proc Natl Acad Sci USA. 2020;117:6323-6329.
- Ma W, Li Y, Chao CYH, et al. Solar-assisted icephobicity down to -60°C with superhydrophobic selective surfaces. Cell Rep Phys Sci. 2021:2:100384.
- Hou Y, Yu M, Shang Y, et al. Suppressing ice nucleation of supercooled condensate with biphilic topography. Phys Rev Lett. 2018;120:075902.
- Chen X, Ma R, Zhou H, et al. Activating the microscale edge effect in a hierarchical surface for frosting suppression and defrosting promotion. Sci Rep. 2013;3:2515.

- 32. Wen R, Ying Y, Ma X, Yang R. Sustainable anti-frosting surface for efficient thermal transport. Cell Rep Phys Sci. 2022;3:100937.
- Lu C, Liu C, Yuan Z, et al. Gradient droplet distribution promotes spontaneous formation of frost-free zone. Commun Mater. 2022;3:80.
- 34. Hao Q, Pang Y, Zhao Y, Zhang J, Feng J, Yao S. Mechanism of delayed frost growth on superhydrophobic surfaces with jumping condensates: more than interdrop freezing. Langmuir. 2014;30:15416-15422.
- Kim P, Wong T-S, Alvarenga J, Kreder MJ, Adorno-Martinez WE, Aizenberg J. Liquid-infused nanostructured surfaces with extreme anti-ice and anti-frost performance. ACS Nano. 2012;6:6569-6577.
- Sarma J, Guo Z, Dai X. Bioinspired photocatalytic hedgehog coating for super liquid repellency. Mater Chem Front. 2021;5:4174-4181.
- Zhao Y, Wang R, Yang C. Interdroplet freezing wave propagation of condensation frosting on micropillar patterned superhydrophobic surfaces of varying pitches. Int J Heat Mass Transfer. 2017;108: 1048-1056
- Seo D, Oh S, Moon B, et al. Influence of lubricant-mediated droplet coalescence on frosting delay on lubricant impregnated surfaces. Int J Heat Mass Transfer. 2019;128:217-228.
- Chatterjee R, Beysens D, Anand S. Delaying ice and frost formation using phase-switching liquids. Adv Mater. 2019;31:1807812.
- Varanasi KK, Deng T, Smith JD, Hsu M, Bhate N. Frost formation and ice adhesion on superhydrophobic surfaces. Appl Phys Lett. 2010:97:234102.
- 41. Rykaczewski K, Anand S, Subramanyam SB, Varanasi KK. Mechanism of frost formation on lubricant-impregnated surfaces. Langmuir. 2013:29:5230-5238.
- 42. Sarma J, Zhang L, Guo Z, Dai X. Sustainable icephobicity on durable quasi-liquid surface. Chem Eng J. 2022;431:133475.
- Guo Z, Zhang L, Monga D, Stone HA, Dai X. Hydrophilic slippery surface enabled coarsening effect for rapid water harvesting. Cell Rep Phys Sci. 2021;2:100387.
- 44. Leng X, Sun L, Long Y, Lu Y. Bioinspired superwetting materials for water manipulation. Droplet. 2022;1:139-169.
- Yang X, Qi B, Lu Y, Zhang W, Wang X. Bionic surface diode for droplet steering. Droplet. 2023;2:e46.
- Zhang L, Guo Z, Sarma J, Dai X. Passive removal of highly wetting liquids and ice on quasi-liquid surfaces. ACS Appl Mater Interfaces. 2020;12:20084-20095.

SUPPORTING INFORMATION

Additional supporting information can be found online in the Supporting Information section at the end of this article.

How to cite this article: Sarma J, Monga D, Guo Z, Chen F, Dai X. Coarsening droplets for frosting delay on hydrophilic slippery liquid-infused porous surfaces. Droplet. 2024;3:e106. doi:10.1002/dro2.106